Silicon (2017) 9:503–509
DOI 10.1007/s12633-014-9248-5

ORIGINAL PAPER

Characterization of New Categories of Bioactive Based Tellurite and Silicate Glasses

G. El-Damrawi · H. Doweidar · H. Kamal

Received: 16 February 2014 / Accepted: 15 September 2014 / Published online: 10 October 2014

Abstract New types of tellurite glass ceramics were prepared and studied from the viewpoint of bioactivity. The obtained results were compared with those of silicate glass ceramics. The crystallization behaviors of both silicate and tellurite glass ceramics with equal ratio of CaO/P_2O_5 were investigated. The silicate glass samples were transformed to glass ceramics by a thermal treatment process. While the tellurite glass ceramics were directly obtained without any thermal treatment. The microstructure of these materials was characterized by X-ray diffraction (XRD), Fourier transform infrared absorption spectroscopy (FTIR) and a scanning electron microscope (SEM) equipped with an energy dispersive spectrometer (SEM/EDX). The results revealed clear proof that TeO_2 promoted the nucleation and crystallization processes which led to the formation of different crystalline bio-phases. While the silicate glasses showed a much lower degree of crystallinity than that presented by the tellurite glass ceramics. The crystals of tellurite containing glass were needle- like morphology, which is attributed to the one-dimensional rapid growth of the apatite-tellurite phase. On the other hand, a particle-like morphology is shown in the silicate glass matrix. Bioactivity of the glasses in simulated body fluids (SBF) was investigated. Tellurite containing glass ceramics showed a better bioactivity during the *in vitro* test than that of the silicate one. This was attributed to a great analogous between the morphology of crystals of tellurite glass and the morphology of hydroxyapatite in human bone, since both possess a needle-like morphology.

G. El-Damrawi (✉) · H. Doweidar · H. Kamal
Glass Research Group, Physics Department, Faculty of Science, Mansoura University, Mansoura 35516, Egypt
e-mail: gomaaeldamrawi@gmail.com

Keywords Silicate · Tellurite · Hydroxyapatite · Bioglass · Bioactivity

1 Introduction

Hydroxyapatite (HA) is usually reported as the most promising material for clinical use [1, 2]. However, the poor mechanical properties of (HA) compared to natural bone is considered the most importunate factor that prevents HA to be used for wider applications, especially for load-bearing implants [3, 4]. On the other hand, bioactive glasses and glass ceramics have been reported to be used as bone graft or fillers. This may due to their ability to form a direct bond to living bone [5, 6].

Addition of fluorides, for example LiF, ZnF_2, NaF and CaF_2 were studied previously by full replacement of silica by borate in the patented Hench's bioglass [14]. Borate glasses have been used in various biomedical applications despite the fact of their low chemical durability [7, 8]. Borate composition as a biomedical material when immersed in phosphate solutions, particles of borate glass were generally dissolved and a layer of hydroxyapatite is precipitated [7, 8].

Bioactive silicate glass-ceramics were reported to be of great importance from the viewpoint of biomedical applications [7], since bonding to bone by using some of polycrystalline silicate glass ceramics was reported previously [8]. On the other hand, the development of new biomaterials has recently concentrated on silica free glasses [9]. This may be because apatite phases (bioactive mineral phase) in silicate glasses were hardly crystallized by promoting adequate conditions such as a heat treatment process and /or adding some activator agents [10–12]. As a result, precipitation of apatite crystals in the as-prepared silicate network were found to be limited [13]. But on the other

hand, silica free glasses such as tellurite and tellurosilicate glasses with specific CaO/P_2O_5 molar ratio exhibits a high tendency for crystallization. The ceramic glasses in this situation were found to contain bioactive phases of composition and structure resembling that of natural bone tissues [14].

Considerable interest of apatite based glass ceramics has extended for orthopedic and dental applications [1–4]. This is because the biocompatibility and bone bonding ability of these materials resulting in the growth of healthy tissues directly on to their surfaces. Several combinations between apatite and other glass phases have been proposed in order to improve the poor mechanical properties of the apatite. Among them, apatite $Ca_5(PO_4)_3$ – wollastonite ($CaSiO_3$) or $CaTeO_3$ have been recommended to be used as clinically bone-repairing materials [15, 16]. In addition, fluorapatite [Ca_5 $(PO_4)_3F$] - wollastonite containing glass ceramics is reported as an accepted type of glass ceramic system which is promising in biomedicine. This type is used for joint prostheses and dental roots [17, 18].

Most of the previous studies are concentrated on silicate glasses as bioactive materials. Studies on tellurite glass ceramics, according to our knowledge are limited to be studied. Therefore, this work will concentrate on the preparation and investigation of a new category of tellurite based glass ceramic and to compare their properties with another category of silicate based glass. Since TeO_2 was reported to be used as an agent for crystallization of apatite and wollastonite phases [19].

2 Materials and Methods

2.1 Preparation of the Glasses

Glasses and glass ceramics were prepared according to the formula $50TeO_2$-$26Na_2O$-$21CaO$-$3P_2O_5$ mol %, given a code G_1(50Te) and $50SiO_2$-$26Na_2O$-$21CaO$-$3P_2O_5$ mol % and given a code G_2(50Si). High purity tellurium dioxide, silicon dioxide, reagent-grade calcium carbonate, sodium carbonate and ammonium dihydrogen phosphate were purchased from Sinopharm Chemical Reagent Co. China and are used to obtain the glass compositions. Raw materials were mixed and melted in alumina crucibles in an electrical Lenton furnace 16/5 UAF (England) at temperature 800 − 1400 °C for 1 hour according to the type of prepared sample. The melt was occasionally swirled to assure homogeneity and attainment of thermal and chemical equilibrium.

After refining, the melted glass was poured by pressing the sample between two ceramic plates to yield disc shaped samples. All samples prepared were homogenous, air bubbles-free and stored in desiccators for characterization.

2.2 Scanning Electron Microscope (SEM)

Surface modifications and microstructure of the bioactive glass samples were examined using a scanning electron microscope (SEM). The scanning micrographs were obtained in a Model Philips XL 30 attached with an EDX unit, operated at an accelerating voltage 25 KV, with a magnification up to 400000X and resolution for W. (3.5 nm). For the SEM study, the pieces were gold plated. Glass powder having particles passing a #100 sieve (150 micron) and retained on a #200 sieve (75 micron). All prepared compositions were introduced in Table 1.

2.3 X-ray Diffraction (XRD)

X-ray diffraction patterns for the selected glass samples were obtained in a Philips PW 1729 diffractometer equipped with a compact analyzer system 1840 and 8203A/02 chart recorder. The X-ray investigations were used to confirm the amorphous or crystalline nature of the structure.

2.4 Fourier Transform Infrared Spectra (FTIR)

The bioglass samples were analyzed by FTIR spectroscopy using a spectrometer Bruker FTIR. Spectra were obtained in the wavenumber range of 4000 to 400 cm^{-1} at 2 cm^{-1} resolution. The FTIR analysis was used to characterize various functional groups, most importantly the hydroxyl and phosphate groups. For the FTIR investigation in transmittance absorption mode, the glassy specimens were grinded to a powder, which was mixed with KBr by the ratio 1:100 in weight. The spectra obtained were corrected for the background and dark current noises.

2.5 Preparation of Simulated Body Fluid (SBF)

The bioactivity is not only a material property but also depends on the solution used for *in vitro* tests. Kokubo et al. [20] developed a series of cellular aqueous solutions, which are able to reproduce *in vivo* surface structure changes in bioactive materials. The simulated body fluid (SBF) solution is the closest to human blood plasma that produced the hydroxyapatite layer.

In vitro samples were performed under static conditions soaking in cylindrical bottles with SBF solution and the soaking time was 5 days.

Table 1 Composition of the prepared glass and glass ceramics

Composition (mol%)	TeO_2	SiO_2	Na_2O	CaO	P_2O_5
G_1(50Te)	50	–	26	21	3
G_2(50Si)	–	50	26	21	3

After soaking, the glass pieces were removed from the solution by filtration, washed with de-ionized distilled water in order to remove the soluble inorganic salts, and then dried at room temperature.

3 Results Discussion

Figure 1(a & b) shows XRD spectrum of tellurite glass ceramic and silicate glasses of composition $50TeO_2$-$26Na_2O$-$21CaO$-$3P_2O_5$ (mol %) and $50SiO_2$-$26Na_2O$-$21CaO$-$3P_2O_5$ (mol %), respectively. It can be realized from Fig. 1 that the XRD pattern of TeO_2 containing glass ceramics possesses a sharp diffraction lines superimposed on a wide shoulder extended from $2\theta = 20°$ to 35°. The sharpness of peaks is clearly evident, indicating rich crystallinity in the investigated sample. However, the pattern of the silicate glass exhibits a weak diffraction line spectra. Broadening of the spectral peaks reflects the poor crystallinity of the prepared silicate glass.

The angular locations of the most peaks of the XRD spectrum (Fig. 1b) closely match the standards which indicate that the major crystalline phases are calcium tellurite and sodium tellurite phases [21, 22]. These phases were $CaTeO_3$ (JCPDF 28-0243) and Na_2TeO_3 (JCPDF 83-1778), in association with different calcium phosphate phases such as $Ca_2P_2O_7$ (JCPDS 9-346). These structure groups were reported to be among the most bioactive and biocompatible phases in the matrix of the glass [23, 24].

But the dominant structure of the studied silicate glass is amorphous in nature as reflected from the XRD pattern (Fig. 1a). In terms of bioactivity, the distorted structure would lead to induced hydroxyapatite layer, differs in some extent to the composition and structure from that of natural bone. While crystalline biophases presented by tellurite glasses can precipitate hydroxyapatite with a Ca/P ratio near to that of natural bone mineral (1.67) [25]. In this situation, however, a limited value of crystallinity is found for as-prepared silicate glasses. Adequate degree of crystallinity is enhanced by the effect of thermal treatment, the crystallinity of treated glass is determined quantitatively (65 %) and (90 %) for the as-prepared tellurite glass ceramic. The limited crystallinity for the as-prepared silicate ceramics leads to a limitation of both the strength and the bioactivity of silicate containing glass. But enhanced crystallinity of treated silicate glass and the as-prepared tellurite glass leads to enhanced bioactivity and mechanical properties of the materials, since the well formed crystalline phases play the role of reactivity of the glass [26].

Results based on scanning electron microscope (SEM), (Fig. 2) agree well with that obtained from XRD. Both would confirm the presence of the crystalline structure of the studied material. SEM of the investigated sample indicates that the morphology appears to consist mainly of needles–like crystals, flattened and accumulated splats as well as some little spheroidized and fine particles. These tellurite crystals are present in most of the area of the investigated sample as needles–like crystals. It is noteworthy

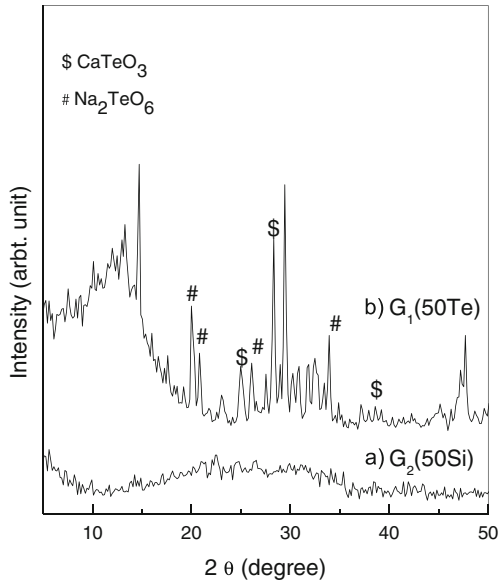

Fig. 1 **a** X-ray diffraction (XRD) pattern of the tellurite glass ceramic of composition ($50TeO_2$-$26Na_2O$-$21CaO$-$3P_2O_5$) mol%, coded as G_1(50Te). **b** (XRD) pattern of the silicate glass of composition ($50SiO_2$-$26Na_2O$-$21CaO$-$3P_2O_5$) mol%, coded as G_2(50Si)

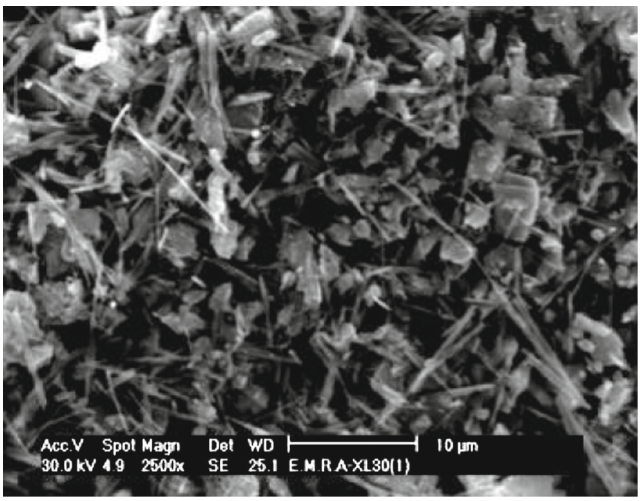

Fig. 2 **a** Scanning electron microscope (SEM) pattern of the tellurite glass of G_1(50Te)

that the morphology of the investigated telluroapatite crystals resembles the morphology of those of human bone and teeth, since the crystalline structure in both cases are needle-like morphology [27, 28]. The latter type of structure was reported to be the most biocompatible and bioactive [29]. It differs from the morphology of silicate glass, where apatite crystals exhibited a particle-like morphology (Fig. 2b).

The EDX spectrum of calcium tellurite rich phase consists of many spectral bands representing Ca, Na and in Te phases. The contents of Ca and Te in the crystalline calcium tellurite phases were evaluated. The obtained atomic ratio of Ca/Te was found to equals 1.04 (Fig. 3a). This value represents crystalline $CaTeO_3$ [30], since the presence of these types was evidenced by previously by XRD. While the EDX spectrum of Ca and P in calcium phosphate rich phases is shown in Fig. 3b. The ratio of spectral bands representing both Ca and P atoms were found to be around unity (1.17) (Fig. 3b). This value characterizes crystalline tri-calcium phosphate phases (TCP) or a mixture of both tri and octa-calcium phosphate phases [31, 32]. These bioactive phases can easily react with simulated body fluid to produce bioactive hydroxyapatite with increased Ca/P ratio to be nearer to value of stable bioactive HA phase, 1.67 [33].

SEM (Fig. 4) as well as XRD data indicates the amorphous nature of the silicate glasses. This could be confirmed by the result based on EDX spectroscopy. The EDX spectrum of the glass is shown in Fig. 5a, b. It can be observed that Si and Ca atoms are considered as the most dominant constituent in the tested sample. The determined atomic ratio of both Ca/Si and Ca/P are 1.09 and 7.03 respectively (Fig. 5a, b). These values were reported to represent wollastonite ($CaSiO_3$) and pseudo apatite [$Ca_5(PO_4)_2SiO_4$] [34, 35]. Accordingly, apatite-wollastonite with the characteristic values given above is considered to be responsible for formation of pseudo amorphous apatite.

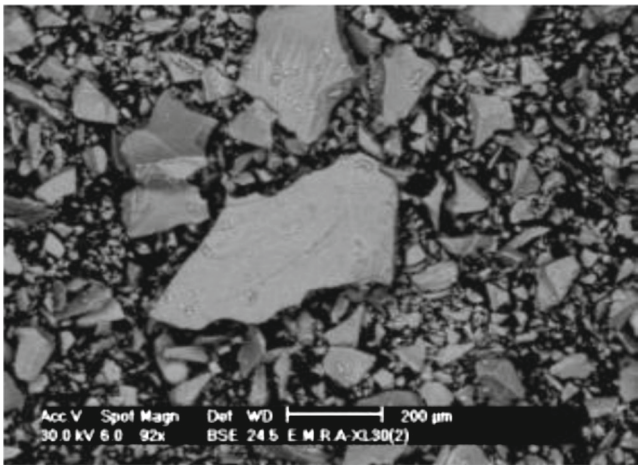

Fig. 4 Scanning electron microscope (SEM) pattern of the silicate glass of G_2(50Si)

Figure 6a shows the Fourier transform infrared absorption spectrum (FTIR) of the investigated tellurite glass in the 1800-400 cm^{-1} range. The spectrum of the prepared pure vitreous TeO_2 is also shown for comparison [19]. The FTIR spectrum of vitreous TeO_2 glass is dominated by two absorption bands at 775 and 660 cm^{-1}. The band at about 775 cm^{-1} is assigned to the Te-O vibration mode in the symmetric equatorial TeO_4 groups. While the broad non-symmetric band at 660 cm^{-1} may represent axial TeO_4 units. Figure 6b shows spectroscopic FTIR in which the addition of Na_2O, P_2O_5 and CaO to TeO_2 glass affects the obtained spectra. The band centered at 660 cm^{-1} in the spectrum of vitreous TeO_2 glass moves to lower wavenumber 600 cm^{-1} in that modified tellurite glass. The weak peaks centered at 700 and 730 cm^{-1} are assigned to mixed stretching ion bending vibration of Te-O-Te bonds overlapped with the bending modes of the phosphate vibrations.

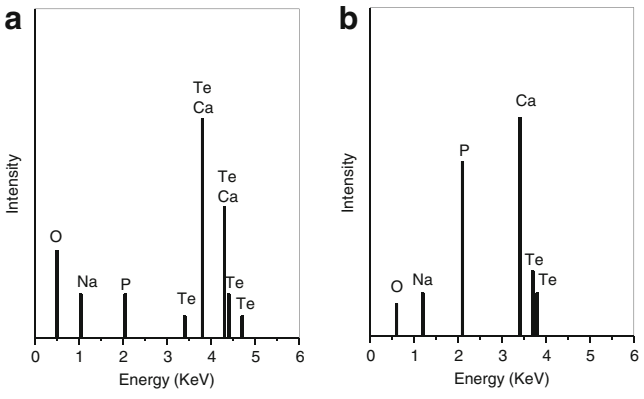

Fig. 3 **a** Energy dispersive X-ray (Edx) pattern of the tellurite glass ceramic of G_1(50Te), Ca/Te =1.04. **b** Energy dispersive X-ray (Edx) pattern of the tellurite glass ceramic of G_1(50Te), Ca/P=1.17

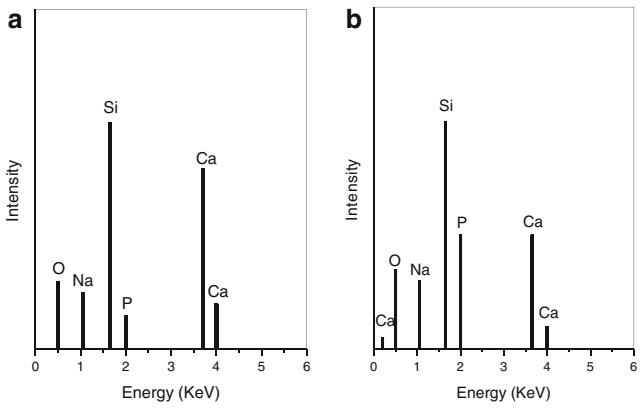

Fig. 5 **a** Energy dispersive X-ray (Edx) pattern of the silicate glass of G_2(50Si), Ca/Si =1.09. **b** Energy dispersive X-ray (Edx) pattern of the silicate glass of G_1(50Te), Ca/P=7.03

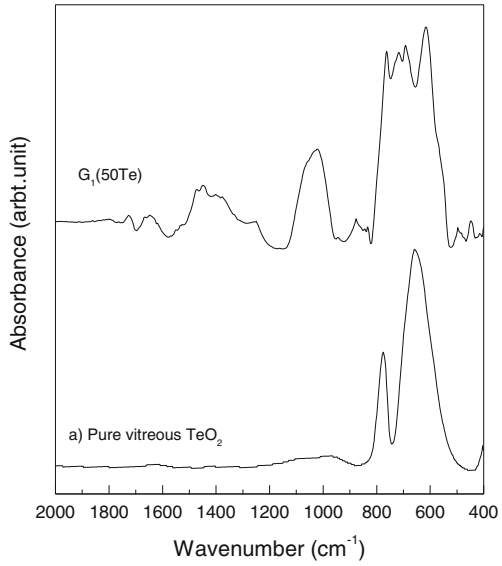

Fig. 6 **a** FTIR spectrum of pure vitreous TeO_2. **b** FTIR spectrum of the G_1(50Te) glass ceramic

The band at 760 cm^{-1} is assigned to the Te-O vibrations in TeO_4 units [36].

It was reported previously [19] that vitreous TeO_4 has a continuous tellurite network and Te atoms are four-coordinated. Addition of modifiers Na_2O and CaO leads to an openness of the glass structure through transformation of TeO_4 units to TeO_3 ones. Disintegration of TeO_4 rings will result in increasing the average atomic ring size through decreasing connectivity (transformation of TeO_4 to TeO_3). The disintegration of TeO_4 rings may be considered as the main reason of broadening of this band. The typical phosphate P-O stretching vibration modes in the crystalline calcium phosphate (apatite) phase are appear around 1048-1097 cm^{-1} [37, 38]. Moreover, the peaks around 505-455 cm^{-1} may reflect the formation of the crystalline apatite [39]. The high frequency bands between 1300 and 1700 cm^{-1} are assigned to segregation and separation of Ca-P phases deposited on the amorphous apatite. Spectral bands between 1456 and 1481 cm^{-1} are reported to be due to distribution of different phosphate sites that depend on nucleation, segregation and formation of apatite crystals [40, 41] which was documented (as discussed previously) by both the XRD and EDX spectra of the investigated telluride glass. The enhanced crystal's field in the presence of Te ions is suggested to play the role of facilitating the crystallization process of dicalcium phosphate. This may give good evidence that TeO_2 containing species can be considered as an agent for crystallization with rates higher than that possessed by silicate structural species.

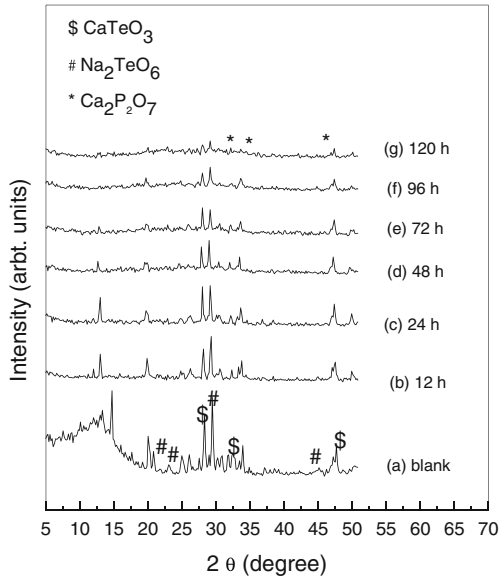

Fig. 7 X-ray diffraction (XRD) patterns of the tellurite glass ceramic of composition before and after soaking in SBF for different time intervals (**a**) to (**g**)

3.1 *In Vitro* Test of Bioactivity

Bioactivity is the property of the material which can be used to develop a direct, adherent and strong bonding with the bone tissue [42]. An *in vitro* test of bioactivity means formation of hydroxyapatite on the material surfaces after suspension in simulated body fluid (SBF). This test has been used as a criterion for the material and determining its bioactivity. *In vivo*, nano-crystals of HA are linked to bioceramic's crystals after implantation. Cell interaction with calcium phosphate bioceramics causes dissolution of the β-TCP releasing Ca^{2+} and PO_4^{-3} onto the microenvironment increasing the super saturation of the biologic fluid with respect to apatite leading to precipitation of the nanocarbonate apatite crystals similar to bone apatite [43–45].

The response of life tissue to bioglass as an implant was found to depend essentially on not only the concentration of crystalline phases developed in the material but also on the Ca/P molar ratio in the crystalline apatite phase. Crystalline apatite with a Ca/P molar ratio around unity is motivated to react with SBF to yield HA with Ca/P molar ratio nearest to 1.67 specified for natural bone tissues [46]. The investigated crystalline phases of the studied material were found to have Ca/P ratio equals to 1.57. In this situation, homogenous HA bone-like structure is predicted to be obtained as a result of interaction of the glass sample with SBF.

Evidently, some reactions between the tested samples and simulated body fluid (SBF) were considered. This can be reflected from the change of spectral bands of XRD of the glasses as the time of immersion changes. Figure 7 shows XRD patterns (a) to (g) of the sample after immersion in SBF at 37 °C for different times of soaking. The characteristic wide XRD peaks of hydroxyapatite (2θ = 32, 40, 46.6

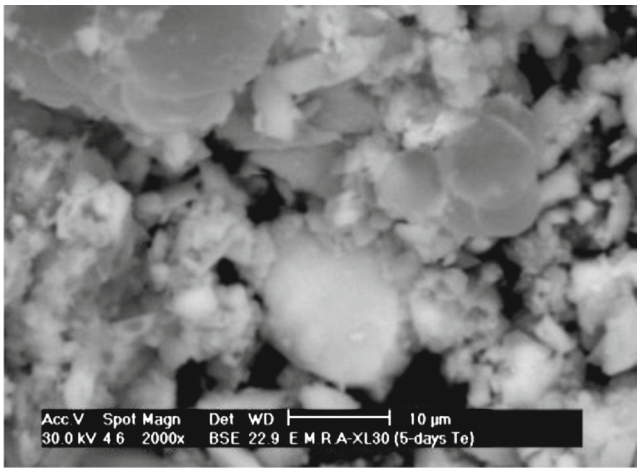

Fig. 8 Scanning electron microscope (SEM) pattern of the silicate glass of G_2(50Si)

and 48) are obviously detected. In addition, the intensity of peaks corresponding to the crystalline calcium tellurite phases decreases gradually with increasing soaking time. At extremely longer time, 120 h, most of these sharp diffraction peaks are mostly not observed. This means that most of the crystallized phases are dissolved during soaking in SBF and the precipitated HA phases that are mutually produced [47–49].

The investigated glasses showed evidence for the mineralization processes. Figure 8 shows that submicron precipitates, enriched in Ca and P (found by EDX –Fig. 9a, b), were uniformly formed after 120 hours, but not earlier (i.e. 72 hours or shorter). Chemical analysis by EDX showed that the sample was rich in P and Ca comparing to the bulk.

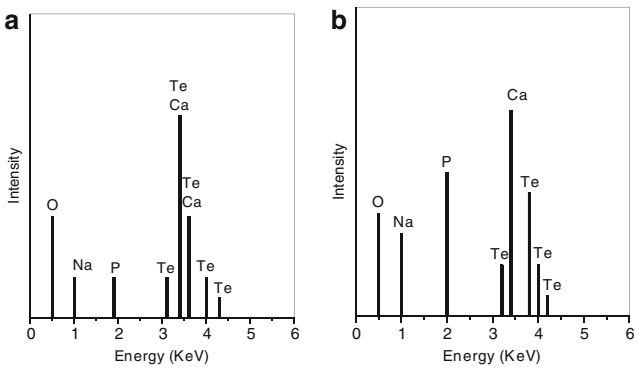

Fig. 9 **a** Energy dispersive X-ray (Edx) pattern of the tellurite glass ceramic of G_2(50Te), Ca/Te=1.09. **b** Energy dispersive X-ray (Edx) pattern of the tellurite glass ceramic of G_1(50Te), Ca/P=1.57

4 Conclusions

Some new categories of tellurite and silicate glass ceramics are prepared and studied from the viewpoint of their bioactivity. The microstructure of these materials was probed by X-ray diffraction (XRD), Fourier transform infrared absorption spectroscopy (FTIR) and a scanning electron microscope (SEM) equipped with an energy dispersive spectrometer (SEM/EDX). It is found that silicate glass samples were transformed to glass ceramics by a thermal heat treatment and sintering processes. While crystalline tellurite glass ceramic is directly obtained from the melt. Silicate glass ceramics showed a much lower degree of crystallinity than that presented by telluride. TeO_2 promoted the nucleation and crystallization processes which led to the formation of different crystalline bio-phases. The crystals of tellurite containing glass were needle-like morphology but particle-like morphology is shown in silicate glass matrix. Bioactivity of the glasses in simulated body fluids (SBF) was investigated. Tellurite containing glass showed a better bioactivity *in vitro* test than that of the silicate one. There is a great analogy between the morphology of crystals of tellurite glass and the morphology of hydroxyapatite in human bone, since both posses needle like morphology. Tellurite glasses are therefore recommended to be used as a bioactive implants and good biodental alternating restorative materials.

References

1. Brandt J, Henning S, Michler G, Hein W, Bernstein A, Schulz M (2010) J of Mater Sci: Mater Med 21:283–294
2. Sona JS, Appleforda M, Onga JL, Wenkeb JC, Kimc JM, Choic SH, Oha DS (2011) J Control Release 153:133–140
3. Roy M, Balla VK, Bose S, Bandyopadhyay A (2010) Advanced Engineering Materials 12:B637–B641
4. Castellania C, Lindtnera RA, Hausbrandta P, Tscheggc E, Tscheggd SE, Zanonie G, Beckf S, Weinberga AM (2011) 7:432–440
5. Nandi SK, Roy S, Mukherjee P, Kundu B, De DK, Basu D (2010) Indian J Med Res 132:15–30
6. Gerhardt LC, Boccaccini AR (2010) Materials 3:3867
7. Rahaman MN, Day DE, Bal BS, Fu Q, Jung SB (2011) Acta Biomater 7:2355
8. Abdelghany A, Kamal H (2014) Ceram Int 40:8003
9. Gutzow I, Schmelzer J (1995) The vitreous state. Springer, Berlin
10. Fokin VM, Zanotto ED (2006) J Non-Cryst Solids 352:2681–2932
11. Lefebvrea L, Chevaliera J, Gremillarda L, Zenatib R, Tholleta G, Assolantc DB, Govinc A (2007) Acta Mater 55:3281–3632
12. Arstila H, Vedel E, Hupa L, Hupa M (2007) J Eur Ceram Soc 27:1543–1546
13. Julian JR (2013) Acta Biomater 9:4457–4486
14. Zaragoza L, Guzmán ER, Gutiérrez LR (2009) J Min Mat Charact Engin 8:591–609

15. Salman SM, Salama SN, Darwish H, Abo-Mosalam HA (2009) Ceram Int 35:1083–1093
16. Chen H, Sun K, Tang Z, Law RV (2006) Cryst Growth Des 6:1504–1508
17. Chakradhara RPS, Nagabhushanab BM, Chandrappab GT, Ramesha KP, Raoc JL (2006) Mater Chem Phys 1:95–169
18. El-Mallawany RA (2012) 2nd edn. CRC Press, Boca Raton
19. Kokubo T, Kushitani H, Sakka S, Kitsugi T, Yamamuro T (1990) J Biomed Mater Res 24:721–734
20. Tagg SL, Huffman JC, Zwanziger JW, Huffman J, Zwanziger J (1994) Chem Mater 6:1884–1889
21. Alias NS, Hussin R, Salim MA (2009) Solid State Sci Technol 17:50–58
22. Mahamid J, Sharir A, Addadi L, Weiner S (2008) Proceedings of the National Academy of Sciences, vol 105, pp 12748–12753
23. Tay FR, Pashley DH, Rueggeberg FA, Loushine RJ (2007) J Endod 33:1347–1351
24. Liu H, Yazici H, Ergun C, Webster TJ, Bermek H (2008) Acta Biomater 4:1472–1479
25. El Damarwi G, Doweidar H, Kamal H (2013) Aust J Basic Appl Sci 7:573–582
26. Xiang Q, Liu Y, Sheng X, Dan X (2007) Dent Mater 23:251–258
27. Zhou H, Lee J (2011) Acta Biomater 7:2769–2781
28. Qiu CF, Xiao XF, Liu RF (2008) Mater Sci Technol 24:612–617
29. Widanarto W, Sahar MR, Ghoshal SK, Arin R, Rohani MS, Effendi M (2013) Mater Lett 108:289–292
30. Crane NJ, Popescu V, Morris MD, Steenhuis P (2006) Bone 39:434–442
31. Pietak AM, Reid JW, Stott MJ, Sayer M (2007) Biomaterials 28:4023–4032
32. Kannan S, Rocha JHG, Ventura JMG, Lemos AF (2005) Scr Mater 53:1259–1262
33. Lu W, Duan W, Guo Y, Ning C (2012) J Biomater Appl 26:637–650
34. George J, Kuboki Y, Miyata T (2006) Biotech Bioeng 95:404–411
35. Rada S, Culea E, Rus V, Pica M, Culea M (2008) J Mater Sci 43:3713–3716
36. Wopenka B, Pasteris JD (2005) Mater Sci Eng 25:131–143
37. Ning CQ, Mehta J, El-Ghannam A (2005) J Mater Sci Mater Med 16:355–60
38. Antonakos A, Liarokapis E, Leventouri T (2007) Biomaterials 28:3043–3054
39. Hoon J, Kang SH (2002) Water Res 36:3925–4176
40. Declercq HA, Verbeeck RMH, Ridder LD (2008) Chem Rev 108:4742
41. LeGeros RZ (2008) Chem Rev 108:4742–4753
42. Li Y, Li D, Weng W (2008) Int J Appl Ceram Technol 5:442–448
43. Nazari AG, Tahari A, Moztarzadeh F, Mozafari M, Bahrololoom ME (2011) Micro Nano Lett 6:713–717
44. Zanotto ED (2013) Int J Appl Glas Sci 4:117–124
45. Olsztaa MJ, Chenga X, Jeea SS, Kumara R, Kima YY, Kaufmane MJ, Douglasa EP, Gowera LB (2007) vol 58, Mater Sci Eng Rep, pp 77–116
46. Dumeliea N, Benhayounea H, Richardb D, Maquinb DL, Balossiera G (2008) Mater Charact 59:129–133
47. Wei M, Ruys AJ, Milthorpe BK, Sorrell CC (2005) Mater Med 16:319–324
48. Anastasios MI, Vaimakis TC (2010) J Therm Anal Calorim 99:785–789
49. Guo X, Xiao P (2006) J Eur Ceram Soc 26:3383–3391